Inorganic Chemistry

Article

pubs.acs.org/IC

Synthesis of Divalent Europium Borate via in Situ Reductive Techniques

Matthew J. Polinski,[‡] Justin N. Cross,[‡] Eric M. Villa,[‡] Jian Lin,[‡] Evgeny V. Alekseev,[§,∥] Wulf Depmeier,[⊥] and Thomas E. Albrecht-Schmitt*[,†]

[†]Department of Chemistry and Biochemistry, 95 Chieftan Way, Florida State University, Tallahassee, Florida 32306-4390, United States

[‡]Department of Chemistry and Biochemistry, University of Notre Dame, Notre Dame, Indiana 46556, United States

[§]Forschungszentrum Jülich GmbH, Institute for Energy and Climate Research (IEK-6), 52428 Jülich, Germany

[∥]Institut für Kristallographie, RWTH Aachen University, D-52066 Aachen, Germany

[⊥]Institut für Geowissenschaften, Universität zu Kiel, 24118 Kiel, Germany

Supporting Information

ABSTRACT: A new divalent europium borate, $Eu[B_8O_{11}(OH)_4]$, was synthesized by two different in situ reductive methodologies starting with a trivalent europium starting material in a molten boric acid flux. The two in situ reductive techniques employed were the use of HI as a source of H_2 gas and the use of a Zn amalgam as a reductive, reactive surface. While both of these are known reductive techniques, the title compound was synthesized in both air and water which demonstrates that strict anaerobic conditions need not be employed in conjunction with these reductive methodologies. Herein, we report on the structure, spectroscopy, and synthetic methodologies relevant to $Eu[B_8O_{11}(OH)_4]$. We also report on a europium doping study of the isostructural compound $Sr[B_8O_{11}(OH)_4]$ where the amount of doped Eu^{2+} ranges from 2.5 to 11%.

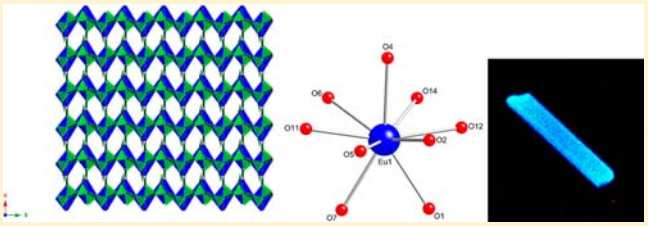

INTRODUCTION

The lanthanide elements exist primarily as trivalent cations in both the solid state and solution, even though additional oxidation states for some lanthanides are known.[1] Europium and ytterbium are the most commonly encountered divalent lanthanides. The stability of the reduced states are often ascribed to the adoption of a half-filled and fully filled 4f shell for Eu^{2+} and Yb^{2+}, respectively.[1] Other divalent lanthanides, such as Sm^{2+}, Nd^{2+}, and Tm^{2+}, are known but those tend to be highly air and moisture sensitive, as well as short-lived.[2−5] Stabilizing the divalent state most often requires the use of soft, highly reducing ligands such as I^-, organic complexes, or using high temperatures with strongly reducing atmospheres.[1,3] Solutions of Eu^{2+} and Yb^{2+} are known to persist for a short amount of time but often oxidize rapidly when exposed to air, especially for the latter. This relative stability is a reflection of the standard reduction potentials ($E°$) for trivalent europium and ytterbium to the divalent species which are −0.35 and −1.05 V, respectively.[1] However, with in the past few years, a number of air and solution stable Eu^{2+} compounds have been reported.[6] For an excellent microreview on Eu^{2+} containing compounds, the interested reader is referred to the work of Allen et al.[7]

Historically, borates have been the subject of interest for their extraordinary optical properties as they are generally transparent into the deep UV and, as such, make excellent host materials for luminescent and nonlinear optical applications.[8−11] When combined with the allowed 4f−5d transition of Eu^{2+} and ensuing luminescence, divalent europium borates represent promising luminescent materials.[12−14] While there is no denying the importance of borates as host materials, our interest in borates stems from a variety of sources with particular emphasis in using borate as a nonredox active and highly polarizable ligand in which to probe the differences in chemistry and reactivity between the lanthanide and actinide elements.[15−21] Borates are among the most structurally diverse polymeric networks and contain BO_3 triangles and/or BO_4 tetrahedra that can corner- or edge-share to form clusters, chains, sheets, or frameworks.[22−24]

The complexity of the borate networks can change as a function of numerous experimental conditions such as pH, temperature, stoichiometry, and complexation to the metal ions. We have recently reported on the structures of several trivalent lanthanide and actinide (i.e., Pu(III), Am(III), and Cm(III)) borate systems that demonstrate the effects that these experimental conditions can have on the resulting structures.[15−17] However, the role that the oxidation state of the lanthanide atoms has on the resulting structures has yet to be fully explored. This is particularly challenging because there are

Received: March 29, 2013
Published: July 3, 2013

dx.doi.org/10.1021/ic400781x | Inorg. Chem. 2013, 52, 8099−8105

very limited options within the lanthanide series for oxidation states other than the trivalent state.[1,3] Of the lanthanides that do deviate from trivalency, stabilizing the other oxidation states in a three-dimensional framework for extended periods of time can be quite difficult.

The photophysical properties of the lanthanides, in particular Eu^{2+}, Eu^{3+}, and Tb^{3+}, have long been explored for their applications in photonics, luminescent probes, light emitting diodes, color rendering properties, and plasma displays.[25] As such, doping studies have long been performed to assess the photochemical properties of these lanthanides within various host materials.[26]

In this work, we report on the structure and properties of a divalent europium borate, $Eu[B_8O_{11}(OH)_4]$, produced from in situ reduction using mild conditions, how the role of a reduced oxidation state effects the resulting structure and properties, and the in situ reductive techniques used to synthesize and stabilize divalent europium within a borate network.

EXPERIMENTAL SECTION

Syntheses. All reactants were of reagent grade and used as received without any further purification: Eu_2O_3 (Alfa Aesar 99.99%), $Eu(CH_3COO)_3{\cdot}xH_2O$ (Alfa Aesar 99%), H_3BO_3 (Alfa Aesar 99.5% min, ACS), $Sr(CH_3COO)_2{\cdot}0.5H_2O$(Alfa Aesar 99.9%), HI (Sigma Aldrich, 57% w/w, unstabilized, 99.99%), Zn shot (99.9% Alfa Aesar), and Hg (99.9% Alfa Aesar).

Two different synthetic methodologies were used in the synthesis of $Eu[B_8O_{11}(OH)_4]$. The first method made use of the generation of reductive H_2 gas upon heating concentrated HI while the second method used a solid zinc/mercury amalgam pellet as a reactive, reductive surface upon which the reactants were added.

For the former method, 200 mg (0.568 mmol) of Eu_2O_3 was charged into a poly(tetrafluoroethylene) (PTFE)-lined Parr 4749 autoclave with a 23 mL internal volume and dissolved using 300 μL of concentrated HI (7.8 M). 0.527 g (8.52 mmol) of boric acid was then added to the sample for a Eu:B molar ratio of 1:15. The above was also performed with a Eu:B molar ratio of 1:30 (0.568 mmol Eu and 17.0 mmol (1.05 g) H_3BO_3). The sample was sealed in a steel autoclave and heated at 240 °C for 5 days under autogenous pressure, which was followed by slow cooling over a 2 day period.

For the latter method, a Zn/Hg amalgam pellet was prepared by dissolving Zn shot into Hg in a glass vial on a hot plate. An approximate ratio of 33%: 67% Zn: Hg(%wt/%wt) was used. Typical amounts were 2.0 g of Zn and 4.0 g of Hg. The molten amalgam was then poured into the Teflon liner to be used directly in the reactions. 64 mg (0.194 mmol) of $Eu(CH_3COO)_3{\cdot}xH_2O$, 0.2481 g (4.01 mmol) of H_3BO_3, and 200 μL of H_2O were loaded into Teflon lined autoclave on top of a Zn amalgam (see SI Figures 1 and 2 in the Supporting Information). The sample was sealed and heated at 200 °C for 24 h and slowly cooled to room temperature over 2 days. The reaction also proceeded when starting with $EuCl_3{\cdot}xH_2O$. Similar attempts using Methyl or Ethyl boronic acid produced a Eu^{2+} borate glass.

In both cases, the resulting product was washed extensively with boiling deionized water to remove the excess boric acid. When using the Zn amalgam, a crystalline byproduct of $ZnB_3O_4(OH)_3$ was observed. Washing was necessary as the product was contained in a solid mass of recrystallized, colorless, and glassy-looking boric acid. Even with repeated washings, it was difficult to completely remove all the remnant borate flux. It should be noted that $Eu[B_8O_{11}(OH)_4]$ is both air and water stable and repeated washings did not dissolve or decompose any of the product. After the washings, the samples were plated onto Petri dishes using either methanol or ethanol and allowed to dry in air which always resulted in some recrystallized boric acid and solid iodine along with the crystalline product. Yields of 71.5% and 64% were obtained for the reactions involving HI and Zn/Hg, respectively.

Synthesis of Eu^{2+} Doped $Sr[B_8(OH)_4O_{11}]$. Doped borate samples were prepared using a modified HI procedure. $Sr_{1-x}[B_8(OH)_4O_{11}]:Eu_x$ samples were prepared with x varied from approximately 0.13 to 0.03 by combining 0.6202 g (10 mmol) of H_3BO_3, 200 μL of concentrated HI, $Sr(CH_3COO)_2{\cdot}0.5H_2O$, and $Eu(CH_3COO)_3{\cdot}xH_2O$ in a Teflon lined autoclave. The amounts of $Sr(CH_3COO)_2{\cdot}0.5H_2O$ and $Eu(CH_3COO)_3{\cdot}xH_2O$ were 96.6 mg and 19.9 mg (0.45 and 0.0606 mmol), 102 mg and 10.0 mg (0.475 and 0.0305 mmol), and 104.7 mg and 5.0 mg (0.4875 and 0.0152 mmol), respectively, which could yield, at most, a doping percentage of 11.9%, 6.0%, and 3.0% Eu^{2+}. Based on atomic percentage of Eu and Sr obtained from the EDX analysis, the average doped amount was 10.3%, 4.1%, and 2.4%, respectively for the reactions listed above. The EDX analysis with atomic percentages can be found in the Supporting Information. The autoclaves were heated at 240 °C for 2 days and slow cooled over 2 days.

Crystallographic Studies. Crystals were mounted on CryoLoops with Krytox oil and optically aligned on a Bruker APEXII Quazar X-ray diffractometer using a digital camera. Initial intensity measurements were performed using an IμS X-ray source, a 30 W microfocused sealed tube (Mo Kα, λ = 0.71073 Å) with high-brilliance and high-performance focusing Quazar multilayer optics. Standard APEXII software was used for determination of the unit cells and data collection control. The intensities of reflections of a sphere were collected by a combination of four sets of exposures (frames). Each set had a different φ angle for the crystal, and each exposure covered a range of 0.5° in ω. A total of 1744 frames were collected with an exposure time per frame of 40 s. SAINT software was used for data integration including Lorentz and polarization corrections. Numerical absorption corrections were applied using the program SCALE (SADABS).[27]

Crystals of $Eu[B_8O_{11}(OH)_4]$ were a two component, non-merohedrally twinned sample with a 180° rotation angle about (10−1). The program CELL_NOW was used to detwin the data. A total of 10,996 reflections were used of which 8476 (77%) were in domain 1 and 6869 (23%) (2449 exclusively) reflections were in domain 2. Multi-Scan absorption corrections were applied using the program SADABS and TWINABS.[27] The structure was solved by direct methods and refined on F^2 by full-matrix least-squares techniques using the program suite SHELX. Solutions were checked using PLATON.[28] Selected crystallographic information is listed in Table 1. Atomic coordinates and additional structural/twinning information are provided in the Supporting Information (CIFs).

Powder diffraction was collected on a Bruker D8 Advance with DaVinci (Cu Kα, λ = 1.5405 Å) using $\theta/2\theta$ geometry. The rotating sample was scanned from 2θ = 5° to 55° at a 0.02 step and 10 s/step.

Table 1. Crystallographic Data for $Eu[B_8O_{11}(OH)_4]$ (EuBO)

mass	478.44
color and habit	colorless, column
space group	$P2_1$
a (Å)	7.6066(2)
b (Å)	8.1217(2)
c (Å)	9.9237(3)
α (deg)	90
β (deg)	108.348(2)
γ (deg)	90
V (Å^3)	581.90(3)
Z	2
T (K)	100(2)
λ(Å)	0.71073
maximum 2θ (deg.)	27.50
ρ_{calcd} (g cm^{-3})	2.731
μ(Mo Kα)	54.79
$R(F)$ for $F_o^2 > 2\sigma(F_o^2)^a$	0.0177
$Rw(F_o^2)^b$	0.0452

$^aR(F) = \sum||F_o| - |F_c||/\sum|F_o|$. $^bR(F_o^2) = [\sum w(F_o^2 - F_c^2)^2/\sum w(F_o^4)]^{1/2}$.

dx.doi.org/10.1021/ic400781x | Inorg. Chem. 2013, 52, 8099−8105

The powder pattern was compared to the calculated pattern and can be found in the Supporting Information (Figure SI 3).

UV−vis−NIR Spectroscopy/Fluorescence. UV−vis−NIR data were acquired for individual crystals using a Craic Technologies microspectrophotometer. Crystals were placed on quartz slides under Krytox oil, and the data were collected from 200 to 1000 nm. The exposure time was auto optimized by the Craic software. Fluorescence data were acquired using the same microspectrophotometer with an excitation wavelength of 365 nm and an exposure time of 1 s.

Infrared Spectroscopy. Infrared spectra were obtained from single crystals using a SensIR technology IlluminatIR FT-IR microspectrometer. Single crystals were placed on quartz IR slides, and the spectrum was collected with a diamond ATR objective. Each spectrum was acquired from 650 to 4000 cm^{-1} with a beam aperture of 100 mm.

Energy-Dispersive Spectroscopy (EDS). Energy-dispersive spectroscopy (EDS) data were collected using a LEO model EVO 50 system with an Oxford INCA energy-dispersive spectrometer. The energy of the electron beam was 20.00 kV, and the spectrum acquisition time was 120 s. All of the data were calibrated with standards, and all EDS results are provided in the Supporting Information. Using three samples from each doped reaction, average doped values of Eu^{2+} were 11.2%, 4.32%, and 2.51% showing a small decrease from the starting doped amounts of 13.5%, 6.4%, and 3.1% respectively.

RESULTS AND DISCUSSION

Structure and Topology Descriptions. $Eu[B_8O_{11}(OH)_4]$ (**EuBO**) crystallizes in the polar, monoclinic space group, $P2_1$. **EuBO** forms a dense, three-dimensional network (Figure 1**a**) that extends in the [*ab*] plane. Figure 2 shows the framework viewed down the *b*-axis where the 2_1 screw and polar axis can be observed. The three-dimensional borate framework is composed of only corner sharing BO_3 triangles and BO_4 tetrahedra. Within the three-dimensional framework, and extending within the [*bc*] plane, are sheets (Figure 1**b**) made up of BO_3 and BO_4 units that create triangular holes in which the europium atoms reside. These triangular holes are composed of nine borate units (four BO_3 and five BO_4 units) of which two BO_3 units and one BO_4 unit edge share to the europium polyhedra. The other borate units within the triangular hole corner share to the europium atom.

Six oxygen atoms are bound in the equatorial plane in a nearly coplanar manner. These oxygen atoms are donated by the borate units of the triangular holes. This forces an unusual geometry not typically observed in f-element chemistry but common in trivalent f-element borate compounds.[15−20] This nine coordinate geometry, known as a hula hoop,[29] is completed by two oxygen atoms from two different BO_3 units on the base sites (O1 and O7) and one oxygen atom from a capping BO_3 unit (O4) (Figure 1**c**).

To achieve three-dimensionality, the sheets must be tethered together to those of the layers above and below. This is accomplished by two different modes of connectivity. The first method uses the capping BO_3 unit (O4) of one europium atom within the sheet. This BO_3 unit is bound to one base site (O1) on the europium atom in the layer above it. The second tethering method comes from the BO_3 unit of the other base site (O7). This unit is bound to the unusual borate trimer containing a μ_3-oxo unit that can be seen within the sheet (Figure 1**b**).

The europium−oxygen bond lengths range from 2.533(5) to 2.722(5) Å for the equatorial oxygen atoms. The base oxygen bond lengths are 2.677(5) and 2.675(4) Å for O1 and O7, respectively, with the capping oxygen bond length at 2.748(5) Å (Table 2). Additionally, O1, O3, O4, and O7 are the hydroxide units and have bond lengths ranging from 2.667(5) to 2.748(5) Å. Bond valence sum (BVS) calculations were also performed based on the bond distances of the oxygen atoms to the europium.[30−33] The BVS calculation yields a bond valence on europium of 2.035.

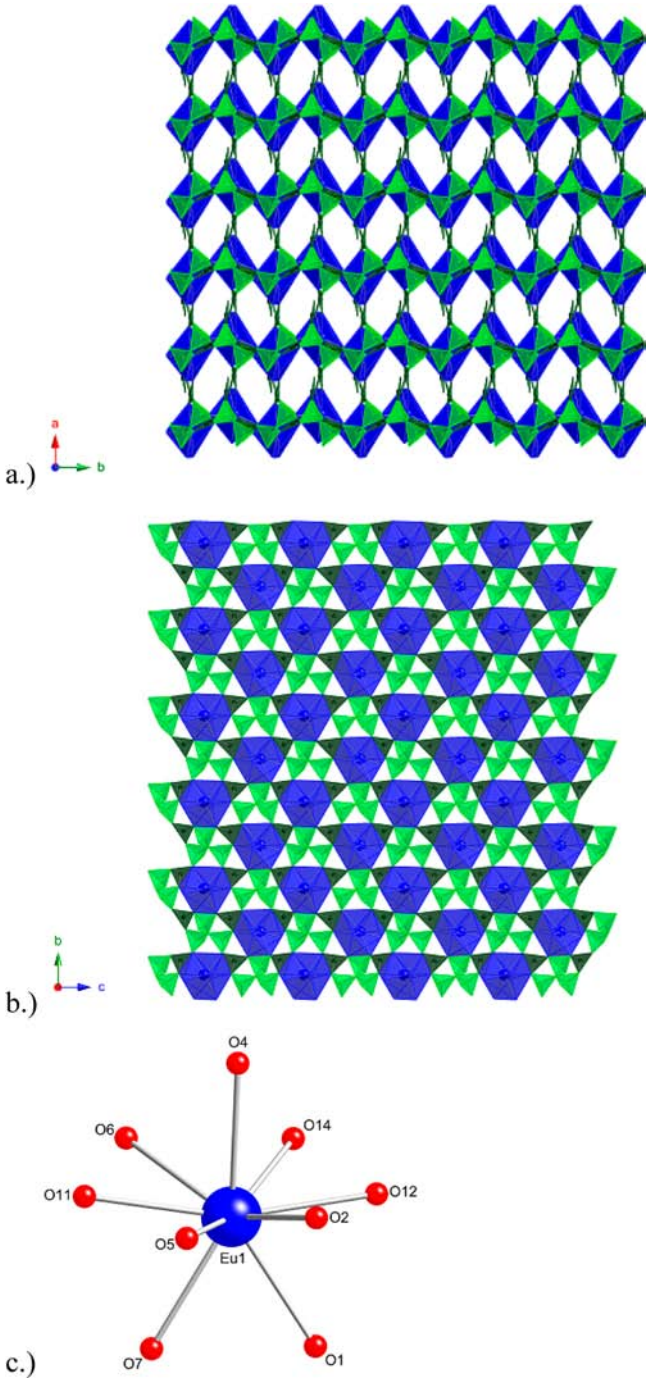

Figure 1. Depiction of the three-dimensional framework (a), sheet topology (b), and hula-hoop coordination geometry (c) about the europium(II) in $Eu[B_8O_{11}(OH)_4]$. The europium is represented by the blue polyhedra, oxygen by red spheres, BO_3 triangles by the dark green polyhedra, and BO_4 tetrahedra by light green polyhedra.

Periodic Trends. $Eu[B_8O_{11}(OH)_4]$ (**EuBO**) has many similarities and differences to other f-element borates that have been prepared. To begin, **EuBO** crystallizes in the polar,

dx.doi.org/10.1021/ic400781x | Inorg. Chem. 2013, 52, 8099−8105

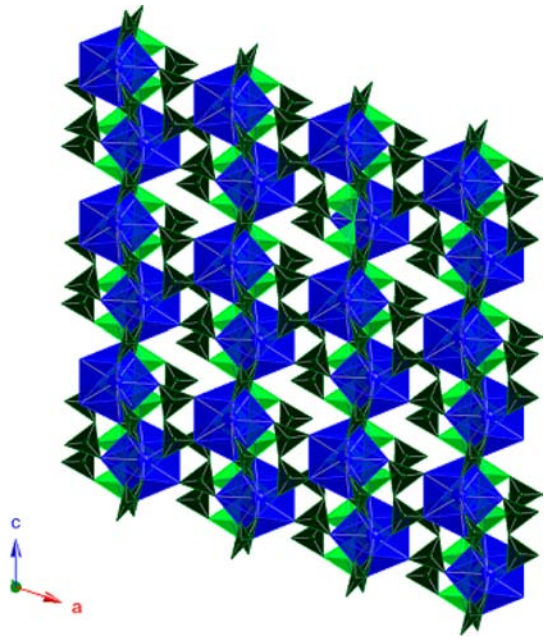

Figure 2. Depiction of the three-dimensional framework as viewed in the [*ac*] plane. The europium is represented by the blue polyhedra, BO_3 triangles by the dark green polyhedra, and BO_4 tetrahedra by light green polyhedra.

Table 2. Selected Bond Distances (Å) for $Eu[B_8O_{11}(OH)_4]$

Eu(1)–O(1)	2.667(5)	B(1)–O(1)	1.366(10)
Eu(1)–O(2)	2.533(5)	B(1)–O(8)	1.364(9)
Eu(1)–O(4)	2.748(5)	B(1)–O(9)	1.382(8)
Eu(1)–O(5)	2.661(5)	B(2)–O(4)	1.370(10)
Eu(1)–O(6)	2.722(5)	B(2)–O(7)	1.364(9)
Eu(1)–O(7)	2.675(4)	B(2)–O(9)	1.381(8)
Eu(1)–O(11)	2.599(4)	B(3)–O(2)	1.453(9)
Eu(1)–O(12)	2.599(5)	B(3)–O(5)	1.446(9)
Eu(1)–O(14)	2.718(5)	B(3)–O(8)	1.446(9)
		B(3)–O(10)	1.537(9)
		B(4)–O(2)	1.369(9)
		B(4)–O(12)	1.376(11)
		B(4)–O(14)	1.366(9)
		B(5)–O(5)	1.366(9)
		B(5)–O(6)	1.361(9)
		B(5)–O(11)	1.383(15)
		B(6)–O(10)	1.502(9)
		B(6)–O(12)	1.452(10)
		B(6)–O(13)	1.466(9)
		B(6)–O(14)	1.449(9)
		B(7)–O(6)	1.446(10)
		B(7)–O(10)	1.509(9)
		B(7)–O(11)	1.441(12)
		B(7)–O(15)	1.465(9)
		B(8)–O(3)	1.368(9)
		B(8)–O(13)	1.366(9)
		B(8)–O(15)	1.368(10)

monoclinic space group $P2_1$. There are no other pure f-element borates that crystallize with that symmetry. In fact, the vast majority of trivalent f-element borates tend to be centrosymmetric.[15−20,34−37] While there are no isotypic or other f-element borates that crystallize in the same space group, **EuBO** is isotypic to $AE[B_8O_{11}(OH)_4]$ (AE = Ca^{2+}, Sr^{2+}).[38,39] The nine-coordinate ionic radii for Eu^{2+} is 1.30 Å while that of Ca^{2+} and Sr^{2+} are 1.18 and 1.31 Å, respectively.[33]

The nine-coordinate geometry about the europium is known as a hula-hoop.[29] This geometry is also observed for other nine-coordinate f-element borates; however, the oxygen donor units on the apical and base sites are different than what has previously been observed.[15−20,34−37] For example, the only other f-element borates with a hula hoop geometry and a BO_3 unit as the capping group are the metal atoms in $Ln[B_9O_{13}(OH)_4]\cdot H_2O$ (Ln = La−Pr, Nd−Eu, Am).[15−20,34] However, in these systems the base sites are composed of oxygen atoms from one edge sharing BO_4 unit. Therefore, the donor ligands on the Eu atoms in **EuBO** are novel in their composition.

The sheet topology observed in **EuBO** is classified as the "M-Type" which is easily identified by the borate trimer formed by the corner sharing of three BO_4 units via a μ_3-oxygen atom (Figure 1**b**).[21] For reference, this sheet topology is also found in a number of other trivalent f-element borate compounds, especially those of the later trivalent actinides.[15−20,34−37] What differentiates the framework of **EuBO** from other f-element borates is in the way the layers are tethered together. There are two different ways in which the sheets are tethered, as described above, and are done so only by BO_3 units. No other trivalent f-element borate compound is connected via only BO_3 units that are present on all the variable coordination sites of the hula hoop (i.e., apical and base positions).

SPECTROSCOPY

Absorbance/Fluorescence. The room temperature absorbance and fluorescence spectra can be seen in Figures 3 and

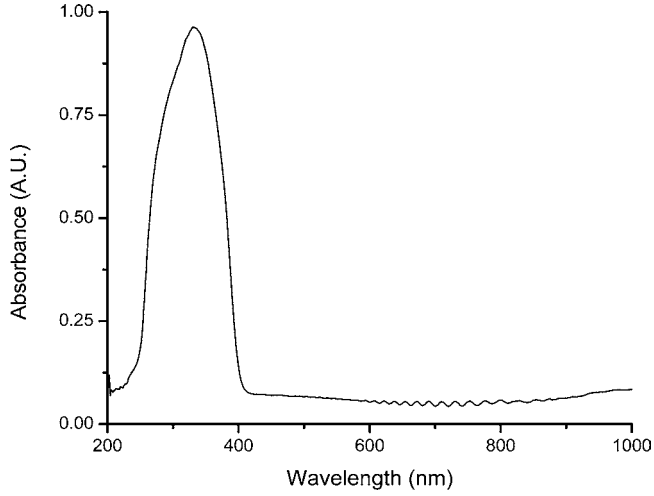

Figure 3. Room temperature absorption data for $Eu[B_8O_{11}(OH)_4]$. The broad absorbance band observed is due to the transition from the ground state ($^8S_{7/2}$) to the $4f^65d$ levels.

4, respectively. The Eu^{2+} ($4f^7$) ion has a ground state term of $^8S_{7/2}$ and very complex energy levels.[40] The complexity arises because of the closeness in energy between the other f^7 excited states and the f^6d states.[41] The broad absorbance band observed in Figure 3 is due to the transition from the ground state to the $4f^65d$ levels. As the $4f^7$ ($^8S_{7/2}$) → $4f^65d$ transition is parity (Laporte) allowed, this transition can be 10^6 times more intense than the parity forbidden f-f transitions.[41,42] As such, it is often characteristic of Eu^{2+} compounds to only observe the

dx.doi.org/10.1021/ic400781x | *Inorg. Chem.* 2013, 52, 8099−8105

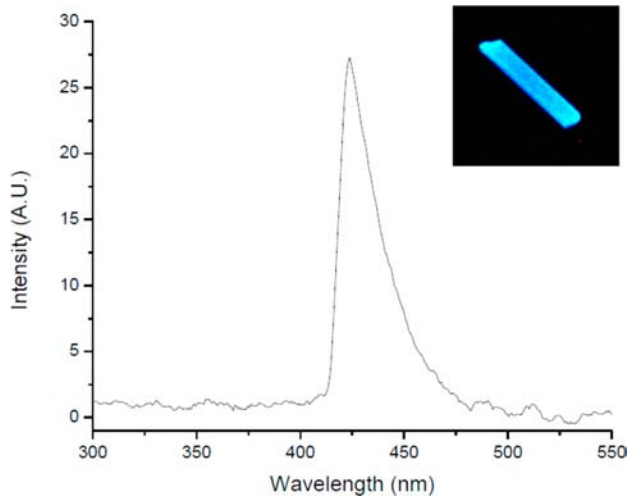

Figure 4. Fluorescence spectrum of $Eu[B_8O_{11}(OH)_4]$ showing the emission near 430 nm and giving off blue light (inset) upon excitation of 365 nm light.

intense, large, and broad charge-transfer band in the UV-region because of the f-f transitions being masked.

The fluorescence spectrum of **EuBO** can be seen in Figure 4. The characteristic blue emission of Eu^{2+} was observed via excitation with 365 nm light at approximately 430 nm. This emission is the result of the 5d-4f transitions. The broadening of the emission line is a result of the sensitivity of the Eu^{2+} center to its surrounding environment since the 5d orbital is naked. The doped samples produced the same blue emission but intensity was greatly increased. Only a qualitative assessment of intensity was made. The emission peak is known to shift significantly depending on the environment of the europium because of nephelauxetic effects on the 5d orbital and can produce red or green emission.[12,42] The fluoresence spectrum is similar to other Eu^{2+} containing compounds reported.[43]

Infrared Spectroscopy. The Infrared (IR) spectrum of **EuBO** can be seen in Figure 5. Borate vibration bands are generally assigned between 1400−1100 cm^{-1} and 1000−800 cm^{-1} for BO_3 and BO_4, respectively.[44−46] The antisymetric

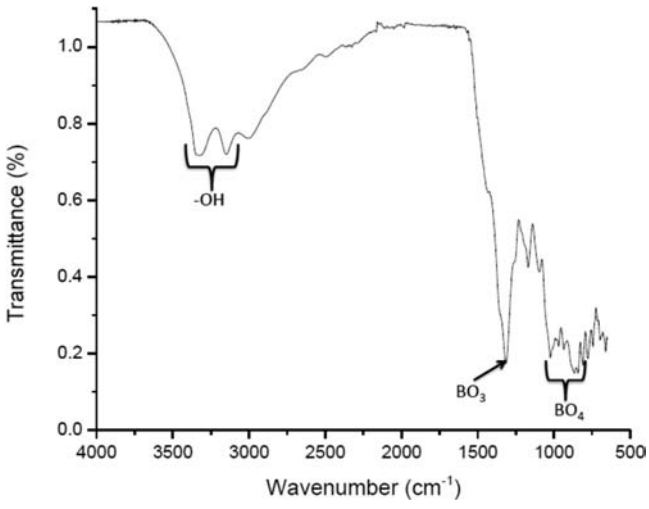

Figure 5. Infrared (IR) spectrum of $Eu[B_8O_{11}(OH)_4]$ with the stretching modes of hydroxide and borate units identified.

stretches observed around 1250 cm^{-1} and 1363 cm^{-1} are consistent with the presence of BO_3 units while the bands clustered around 800 cm^{-1} are consistent with the presence of BO_4 units (Figure 5).[44−46] The IR spectrum also indicates the presence of bound hydroxide units with the stretches near 3250 cm^{-1} and the absence of water based on the lack of the bending stretch near 1610−1620 cm^{-1}.

SYNTHETIC METHODOLOGY

$Eu[B_8O_{11}(OH)_4]$ was synthesized starting with Eu_2O_3 and $Eu(CH_3COO)_3{\cdot}xH_2O$ via two different in situ reductive techniques. The first technique made use of the decomposition of HI(aq) into H_2(g) and I_2(s) during heating. The release of hydrogen gas provides a reducing hydrogen atmosphere within the sealed Teflon liner. Under the experimental conditions discussed above, the presence of a hydrogen atmosphere provides enough of a reducing environment to reduce Eu^{3+} to Eu^{2+} ($E°$ = −0.35 V). While reduction potentials are measured under standard conditions, we can only use them as a guide. The second technique made use of a Zn amalgam as a reactive reductive surface that is present in the Teflon liner throughout. Zn amalgam has a reductive potential of 0.7618 V that is well above the potential needed to reduce Eu^{3+} to Eu^{2+} at standard temperature and pressure (STP).[47] As mentioned before, these systems are far away from STP, and these potentials can only be used as a guide. The use of metal amalgams for reducing ions in solutions has been known for quite some time but the formation of the title compound under the experimental conditions discussed above proves that the same technique can be used at elevated temperatures and in boric acid flux reactions. This makes it a flexible technique to access oxidation states that are not typically seen in these types of reactions.

The success of the doping study shows a proof of concept for producing Eu^{2+} phosphors using these new techniques. The doping amount can be easily and reliably varied as shown by the EDS data. Clean reduction of Eu^{3+} to Eu^{2+} still occurred in these reactions even at shortened reaction times and slightly lowered temperatures. This could prove to be a facile method of producing Eu^{2+} phosphors that does not rely on the typical scheme of high temperature solid state techniques with rigorous exclusion of oxygen.

It is important to note two things about both in situ reductive techniques. The first is that the box furnace in which these reactions were conducted are *not* in an Ar/inert atmosphere glove boxes and all manipulations were performed on a benchtop with no regard to air and water exclusion. As the Teflon liners are not impervious to oxygen, oxygen can never be fully excluded. Second, adding both HI and boric acid allows for water to be present. As such, both of these methods provide means of reducing europium when both oxygen and water are present in the reaction conditions. Additionally, this compound is both air and water stable and does not appear to be oxidized after the compound has been obtained. As of the date of this writing, it has been nearly 9 months post-synthesis. Both crystallographic and spectroscopic analyses do not give any indication of oxidation to Eu^{3+}.

CONCLUSIONS

There are many similarities and differences between the chemistry of Eu^{2+} and other Ln^{3+} borates. While a common sheet topology is observed, the coordination to the metal atom is rather novel and allows for the crystallization in a polar,

dx.doi.org/10.1021/ic400781x | *Inorg. Chem.* 2013, 52, 8099−8105

noncentrosymmetric space group. The ionic radius of Eu^{2+} with a coordination number of nine is 1.30 Å.[33] This is much large than some other Ln^{3+}/An^{3+} cations that adopt a ten-coordinate geometry, yet Eu^{2+} prefers the lower coordination environment. Additionally, Eu^{2+} is much softer than other Ln^{3+}/An^{3+} cations and yet it elects to exclude iodine from the structure. There are several examples of trivalent lanthanide borates that have iodine bound to the metals.[18,20]

We have synthesized a divalent europium borate compound via two in situ reductive techniques. The use of both concentrated HI(aq), in the first, and a Zn amalgam, in the second, directly in the reaction vessel allows for the formation of a pure divalent oxidation state compound. Additionally, these methods provide means for reductive chemistry in hydrothermal conditions when exposed to both air and water. We feel that these techniques can be applied to other systems to yield reduced metal compounds in either unusual or less common oxidation states. Investigations into other ligand systems and metals are currently underway.

■ ASSOCIATED CONTENT

Supporting Information

X-ray crystallographic data in CIF format and the EDS spectra. This material is available free of charge via the Internet at http://pubs.acs.org.

■ AUTHOR INFORMATION

Corresponding Author

*E-mail: talbrechtschmitt@gmail.com.

Notes

The authors declare no competing financial interest.

■ ACKNOWLEDGMENTS

We are grateful for support provided by the Chemical Sciences, Geosciences, and Biosciences Division, Office of Basic Energy Sciences, Office of Science, Heavy Elements Chemistry Program, U.S. Department of Energy, under Grant DE-FG02-09ER16026, which supports all of the synthetic, structural, and spectroscopic studies as well as support provided by the Materials Science of Actinides, an Energy Frontier Research Center funded by the U.S. Department of Energy, Office of Science, Office of Basic Energy Sciences under Award Number DE-SC0001089. Collaborative work with our German counterparts is supported via the Helmholtz Association, Grant No. VH-NG-815.

■ REFERENCES

(1) Cotton, S. *Lanthanide and Actinide Chemistry*; John Wiley and Sons, Ltd.: Chichester, U.K., 2006.

(2) Meyer, G. *Chem. Rev.* **1988**, *88*, 93.

(3) Morss, L. R. *Chem. Rev.* **1976**, *76*, 827.

(4) Evans, W. J. *Inorg. Chem.* **2007**, *46*, 3435−3449.

(5) MacDonald, M. R.; Bates, J. E.; Fieser, M. E.; Ziller, J. W.; Furche, F.; Evans, W. J. *J. Am. Chem. Soc.* **2012**, *20*, 8420−8423.

(6) (a) Gamage, N.-D. H.; Mei, Y.; Garcia, J.; Allen, M. J. *Angew. Chem., Int. Ed.* **2010**, *49*, 8923−8925. (b) Garcia, J.; Neelavalli, J.; Haacke, E. M.; Allen, M. J. *Chem. Commun.* **2011**, *47*, 12858−12860. (c) Garcia, J.; Kuda-Wedagedara, A. N. W.; Allen, M. J. *Eur. J. Inorg. Chem.* **2012**, 2135−2140.

(7) Garcia, J.; Allen, M. J. *Eur. J. Inorg. Chem.* **2012**, 4550−4563.

(8) (a) Giesber, H.; Ballato, J.; Chumanov, G.; Kolis, J.; Dejneka, M. *J. Appl. Phys.* **2003**, *93*, 8987. (b) Giesber, H.; Ballato, J.; Pennington, W. T.; Kolis, J. W.; Dejneka, M. *Glass Technol.* **2003**, *44*, 42.

(9) Saubat, B.; Fouassier, C.; Hagenmuller, P.; Bourcet, J. C. *Mater. Res. Bull.* **1981**, *16*, 193−198.

(10) Machida, K.; Adachi, G.; Shiokawa, J. *J. Lumin.* **1979**, *21*, 101−110.

(11) Pei, Z. W.; Su, Q.; Zhang, J. Y. *J. Alloys Compd.* **1993**, *198*, 51−53.

(12) Höppe, H. A. *Angew. Chem., Int. Ed.* **2009**, *48*, 3572−3582.

(13) Machida, K.; Hata, H.; Okuno, K.; Adachi, G.; Shiokawa, J. *J. Inorg. Nucl. Chem.* **1979**, *41*, 1425−1430.

(14) Schipper, W. J.; van der Voort, D.; van den Berg, P.; Vroon, Z. A. E. P.; Blasse, G. *Mater. Chem. Phys.* **1993**, *33*, 311−317.

(15) Polinski, M. J.; Wang, S.; Alekseev, E. V.; Depmeier, W.; Albrecht-Schmitt, T. E. *Angew. Chem., Int. Ed.* **2011**, *50*, 8891−8894.

(16) Polinski, M. J.; Wang, S.; Alekseev, E. V.; Depmeier, W.; Liu, G.; Haire, R. G.; Albrecht-Schmitt, T. E. *Angew. Chem., Int. Ed.* **2012**, *51*, 1869−1872.

(17) Polinski, M. J.; Grant, D. J.; Wang, S.; Alekseev, E. V.; Cross, J. N.; Villa, E. M.; Depmeier, W.; Gagliardi, L.; Albrecht-Schmitt, T. E. *J. Am. Chem. Soc.* **2012**, *134*, 10682−10692.

(18) Polinski, M. J.; Wang, S.; Cross, J. N.; Alekseev, E. V.; Depmeier, W.; Albrecht-Schmitt, T. E. *Inorg. Chem.* **2012**, *51*, 7859−7866.

(19) Polinski, M. J.; Wang, S.; Alekseev, E. V.; Cross, J. N.; Depmeier, W.; Albrecht-Schmitt, T. E. *Inorg. Chem.* **2012**, *51*, 11541−11548.

(20) Polinski, M. J.; Alekseev, E. V.; Darling, V. R.; Cross, J. N.; Depmeier, W.; Albrecht-Schmitt, T. E. *Inorg. Chem.* **2013**, *52*, 1965−1975.

(21) Wang, S.; Alekseev, E. V.; Depmeier, W.; Albrecht-Schmitt, T. E. *Chem. Commun.* **2011**, *47*, 10874−10885.

(22) Burns, P. C.; Grice, J. D.; Hawthorne, F. C. *Can. Mineral.* **1995**, *33*, 1131.

(23) Grice, J. D.; Burns, P. C.; Hawthorne, F. C. *Can. Mineral.* **1999**, *37*, 731.

(24) Yuan, G.; Xue, D. *Acta Crystallogr.* **2007**, *B63*, 353.

(25) (a) Wang, J. F.; Wang, R. Y.; Yang, J.; Zheng, Z. P.; Carducci, M. D.; Cayou, T. J. *J. Am. Chem. Soc.* **2001**, *123*, 6179−6180. (b) Jang, H.; Shin, C. H.; Jung, B. J.; Kim, D. H.; Shim, H. K.; Do, Y. *Eur. J. Inorg. Chem.* **2006**, 718−725. (c) Bünzli, J.-C. G.; Eliseeva, S. V. *Chem. Soc. Rev.* **2010**, *39*, 189−227. (d) Jiang, Y. D.; Zhang, F.-L.; Summers, C. J.; Wang, Z. L. *Appl. Phys. Lett.* **1999**, *74*, 1677−1679.

(26) Bünzli, J.-C. G.; Piguet, C. *Chem. Soc. Rev.* **2005**, *34*, 1048−1077.

(27) Sheldrick, G. M. *SADABS, Program for absorption correction using SMART CCD based on the method of Blessing*; Bruker AXS: Madison, WI, 2001. Blessing, R. H. *Acta Crystallogr.* **1995**, No. A51, 33.

(28) Spek, A. L. *J. Appl. Crystallogr.* **2003**, *36*, 7−13.

(29) Ruiz-Martínez, A.; Casanova, D.; Alvarez, S. *Chem.—Eur. J.* **2008**, *14*, 1291−1303.

(30) Brown, I. D.; Altermatt, D. *Acta Crystallogr.* **1985**, *B41*, 244−247.

(31) Brese, N. E.; O'Keeffe, M. *Acta Crystallogr.* **1991**, *B47*, 192−197.

(32) Brown, I. D. *Chem. Rev.* **2009**, *109*, 6858−6919.

(33) Shannon, R. D. *Acta Crystallogr., Sect. A* **1976**, *32*, 751−767.

(34) Belokoneva, E. L.; Stefanovich, S.; Dimitrova, O. V.; Ivanova, A. G. *Zh. Neorg. Khim.* **2002**, *47*, 370−377.

(35) Li, L.; Jin, X.; Li, G.; Wang, Y.; Liao, F.; Tao, G.; Lin, J. *Chem. Mater.* **2003**, *15*, 2253−2260.

(36) Lu, P.; Wang, Y.; Lin, J.; You, L. *Chem. Commun.* **2001**, 1178−1179.

(37) Li, L.; Lu, P.; Wang, Y.; Jin, X.; Li, G.; Wang, Y.; You, L.; Lin, J. *Chem. Mater.* **2002**, *14*, 4963−4968.

(38) Yamnova, N. A.; Tismenko, E.; Yu., K.; Zubkova, N. V.; Dimitrova, O. V.; Kantor, A. P. *Kristallografiya.* **2005**, *5*, 827−833.

(39) Brovkin, A. A.; Zayakina, N. V.; Brovkina, V. S. *Kristallografiya.* **1975**, *5*, 563−566.

(40) Jiang, J.; Higashiyama, N.; Machida, K.; Adachi, G. *Coord. Chem. Rev.* **1998**, *170*, 1−29.

(41) *Physics of Laser Crystals*; Krupa, J.-C., Kulagin, N. A., Eds.; Kluwer Academic Publishers: Dordrecht, The Netherlands, 2003.

(42) (a) Song, H.; Lu, S.; Renxi Gao, S. E.; Zhang, J.; Chen, B.; Xia, H.; Zhang, J.; Ni, Q. *J. Appl. Phys.* **2002**, *91*, 2959−2964. (b) Lawson, J. K.; Payne, S. A. *Phys. Rev. B* **1991**, *47*, 14003−14010.
(43) (a) Xia, Z.; Wang, X.; Wang, Y.; Liao, L.; Jing, X. *Inorg. Chem.* **2011**, *50*, 10134−10142. (b) Xia, Z.; Zhuang, J.; Liu, H.; Liao, L. *J. Phys. D: Appl. Phys.* **2012**, *45*, 015302. (c) Herrmann, A.; Fibikar, S.; Ehrt, D. *J. Non-Cryst. Solids* **2009**, *355*, 2093−2101.
(44) Peak, D.; Luther, G. W.; Sparks, D. L. *Geochim. Cosmochim. Acta* **2003**, *67*, 2251−2560.
(45) Chen, X.; Zhao, Y.; Chang, X.; Zuo, J.; Zang, H.; Xiao, W. *J. Solid State Chem.* **2006**, *179*, 3911−3918.
(46) Kazmierczak, K.; Höppe, H. A. *Eur. J. Inorg. Chem.* **2010**, 2678−2681.
(47) *CRC Handbook of Chemistry and Physics*, 85th ed.; CRC Press: Boca Raton, FL, 2004−2005.